American Mineralogist, Volume 74, pages 1124–1129, 1989

Possible sites for protonation in β-Mg_2SiO_4 from an experimentally derived electrostatic potential

JAMES W. DOWNS
Department of Geology and Mineralogy, Ohio State University, Columbus, Ohio 43210, U.S.A.

ABSTRACT

The electrostatic potential for β-Mg_2SiO_4 is derived from the single-crystal X-ray diffraction data of Horiuchi and Sawamoto (1981). A broad minimum in the potential near the underbonded O(1) site indicates this to be a likely site for protonation, corroborating the conclusion of Smyth (1987). However, the minimum in the electrostatic potential for the unit cell is not near the O(1) site, but is located above and below the bonding plane of triangularly coordinated O(2), similar to that observed by Spackman et al. (1987) near the three-coordinated oxygens of stishovite. Therefore, the electrostatic potential indicates O(2) also to be a likely candidate for protonation.

INTRODUCTION

It has been proposed by Smyth (1987) that β-Mg_2SiO_4 could act as a possible host for water in the lower portion of the upper mantle, which would have a profound influence on melting relations and mantle evolution. Smyth's assertion is based on a comparison of Pauling bond-strength sums and ionic-model site potentials among possible mantle phases compiled from the database of Smyth and Bish (1987).

The crystal structure of β-Mg_2SiO_4 was solved by Moore and Smith (1970) from X-ray powder-diffraction data and refined by Horiuchi and Sawamoto (1981) from single-crystal X-ray diffraction intensities. A representation of the crystal structure is shown in Figure 1. Although often referred to as a *modified spinel structure,* the O(2) oxygen is bonded to two tetrahedrally coordinated Si, which would classify this material as a sorosilicate in the traditional Bragg classification scheme (Bragg, 1930). As shown in Figure 1, O(2) is triangularly coordinated to two Si and one Mg and is thus oversaturated ($s = 2.33$) in the strict Pauling sense. However, the Si–O(2) bond distances, 1.703 Å, are among the longest tetrahedral SiO distances known, and the Si–O(2)–Si angle is a very narrow 122.0°.

Figure 1 reveals that O(1) is in approximately square pyramidal coordination to five Mg, yielding a formal Pauling bond-strength sum of only 1.67. As pointed out by Smyth (1987), O(1) is not only underbonded in the Pauling sense but also has a small ionic-model site potential that is typical of an oxygen that could accept a proton to become OH^-. In fact, of 28 oxygens in 11 normally anhydrous high-pressure silicates examined by Smyth (1987), O(1) of β-Mg_2SiO_4 was the only one to meet all of the criteria normally associated with OH^- sites in silicates. The assertion of Smyth is *not* that all O(1) oxygens in β-Mg_2SiO_4 are really OH^-, but rather that such a substitution could occur as a defect when charge-balanced by appropriate M-site vacancies.

An obvious experimental test for the presence of OH^- in β-Mg_2SiO_4 is to examine the O–H stretching region of vibrational spectra. Raman spectra in the high-energy region were reported by McMillan et al. (1987), who found a major O–H stretching peak at 3322 cm^{-1} with an associated shoulder at 3358 cm^{-1} that they ascribed to possible protonation at O(1). However, recent work by McMillan (personal communication) reveals bands assigned to H–O–H bending indicating that the O–H stretching modes may in fact be due to molecular water. This finding however does not invalidate Smyth's identification of O(1) as a likely site for protonation.

The analysis carried out by Smyth (1987) was completed by assuming a simple ionic model with full ionic charges of Si^{4+}, Mg^{2+}, and O^{2-}. Although ionic-model calculations have proven useful for a wide variety of rock-forming minerals (cf. Burnham, 1985), it is desirable to search for theoretical or experimental methods that rely on the actual charge distribution, making no assumptions concerning the nature of chemical bonding in the material. The ideal, but currently impractical, solution would be to solve accurately the nonrelativistic Schrödinger equation for the nonhydrous and protonated forms of β-Mg_2SiO_4 and learn directly about the energetics that accompany the protonation process. Another approach would be to examine protonation of appropriate molecular clusters extracted from the crystalline environment by ab initio self-consistent-field (SCF) calculations using large basis sets.

Aside from using quantum mechanical methods to calculate the protonation energy, insight into protonation processes can be obtained through examination of the *electrostatic potential,* $\phi(\mathbf{r})$, given by

$$\phi(\mathbf{r}) = \sum_a Z_a |\mathbf{R}_a - \mathbf{r}|^{-1} - \int \rho(\mathbf{r}') |\mathbf{r}' - \mathbf{r}|^{-1} \, d\tau, \quad (1)$$

0003–004X/89/0910–1124$02.00

where Z_a is the charge on nucleus a, R_a refers to a nuclear coordinate, and $\rho(\mathbf{r})$ is the electron density (Politzer and Truhlar, 1981). The first term refers to the nuclear charge distribution, and the second term to the electron distribution. The electrostatic potential is simply tlhe first inner moment of the total charge distribution or the convolution of the total charge density onto $|\mathbf{r}' - \mathbf{r}|^{-1}$. The electrostatic potential represents the total electric potential field at $\mathbf{r}$ arising from the unperturbed total charge distribution. Maps of the electrostatic potential are normally plotted in units of e/Å (1 e/Å = 14.40 eV/unit charge = 1389 kJ/mol charge = 332.1 kcal/mol charge). For example, if the value of the electrostatic potential at a particular point is -0.1 e/Å, this means that a positive test charge starting from infinity would acquire 1.44 eV in energy in arriving at that point.

The electrostatic potential has proven useful in the study of protonation processes since it is a measure of the attraction of a proton toward a charge distribution (Tomasi, 1981). Its usefulness has been tested against Hartree-Fock limit SCF calculations on molecules where the total interaction energy between the molecule and proton is determined. Tomasi (1981) has shown that even though polarization and charge-transfer terms may account for more than 50% of the total interaction energy, the electrostatic term follows the same trend as the total energy. Tomasi (1981) has reported an excellent correlation between the electrostatic potential at protonation sites of molecules and protonation energies obtained from calculations at the Hartree-Fock limit. These tests have shown that the electrostatic potential can be used to predict the geometry of a protonated molecule and the relative energies of different protonation sites on the same molecule. In other words, the location of the electronegative minima in a map of the electrostatic potential may be used to predict protonation sites. If several such minima occur, the one with the deepest potential is expected to be the most likely candidate for protonation.

If the protonation process involves lone pairs, it has been shown that SCF calculations that are less than Hartree-Fock limit quality may have considerable errors (Tomasi, 1981). However, since even SCF calculations that approach Hartree-Fock quality tend to yield accurate one-electron properties, such as the electron density and electrostatic potential, the electrostatic potential approach may be the favored method for studying protonation processes when calculations with a complete basis set are intractable. This tends to be the case for large systems containing second-row atoms such as β-Mg_2SiO_4.

X-ray structure factors are Fourier components of the mean thermal one-electron density function in the unit cell of a crystal. Just as one can map out the electron density from X-ray structure factors, the electrostatic potential can also be experimentally retrieved from X-ray diffraction data as first shown by Stewart (1979) and as extended to minerals by Spackman and Stewart (1981). Electrostatic-potential studies of minerals include those of quartz, NaF, Si, diamond, and graphite by Stewart (1982), coesite (Geisinger et al., 1987), phenakite (Downs and Gibbs, 1987), stishovite (Spackman et al., 1987), and zeolite A (Spackman and Weber, 1988). Herein is reported the results of an exploratory mapping of the electrostatic potential for β-Mg_2SiO_4 using the published single-crystal X-ray structure factor moduli of Horiuchi and Sawamoto (1981).

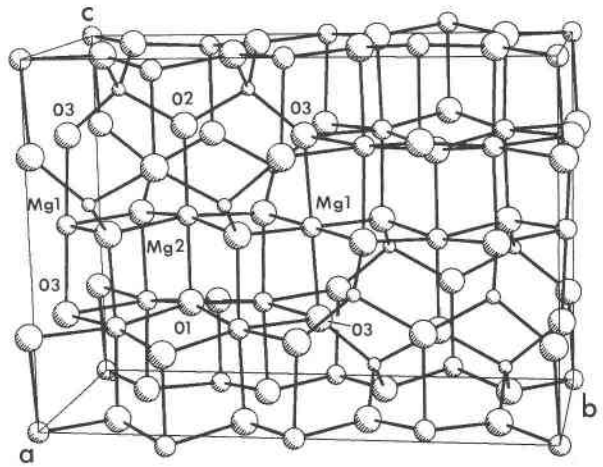

Fig. 1. Crystal structure of β-Mg_2SiO_4. Large, intermediate, and small spheres represent oxygen, Si, and Mg atoms respectively. No significance should be attached to the size of the spheres.

Methods

The retrieval of the electrostatic potential, $\phi(\mathbf{r})$, from measured X-ray structure-factor amplitudes is completed using a combination of Fourier-series and direct-space lattice-summation techniques where

$$\phi(\mathbf{r}) = \Delta\bar{\phi}(\mathbf{r}) + \phi_{\mathrm{IAM}} + \phi_0. \quad (2)$$

The first term, $\Delta\bar{\phi}(\mathbf{r})$, is the mean thermal-deformation electrostatic potential and represents the difference between the vibrationally smeared total electrostatic potential and the vibrationally averaged electrostatic potential of a reference model consisting of spherically averaged, neutral atoms. The bar denotes a vibrational average. This reference model is known as the independent-atom model (denoted IAM) and is the electron-density model of choice in most conventional crystal-structure refinements. $\Delta\bar{\phi}(\mathbf{r})$ is evaluated by using a Fourier series (Eq. 3) very similar to that used to represent the vibrationally averaged deformation electron-density $\Delta\bar{\rho}(\mathbf{r})$.

$$\Delta\bar{\phi}(\mathbf{r}) = -(4\pi V)^{-1} \sum_{hkl} (F_{\mathrm{O}} - F_{\mathrm{IAM}}) \exp(-2\pi i \mathbf{H}\cdot\mathbf{r}) (\sin\theta/\lambda)^{-2}. \quad (3)$$

Here, the F_{O} values are the observed structure factors with phases from some electron-density model, F_{IAM} values are structure factors for the independent-atom model, $\mathbf{H}$ is the Bragg vector with $|\mathbf{H}| = 2 \sin\theta/\lambda$, and V is the unit-cell volume.

The only differences between the Fourier-series expres-

sion for $\Delta\bar{\rho}(\mathbf{r})$ and $\Delta\bar{\phi}(\mathbf{r})$ are the constant in front, with minus sign, and the factor of $(\sin\theta/\lambda)^{-2}$. The minus sign simply preserves the sign convention of the electrostatic potential so that a region where there is an accumulation of electron density, relative to the independent-atom model, will be electronegative (i.e., attractive to a proton). The weight of $(\sin\theta/\lambda)^{-2}$ applied to each Fourier coefficient comes from the Fourier transform of $|\mathbf{r} - \mathbf{r}'|^{-1}$ in Equation 1 as demonstrated by Spackman and Stewart (1981). The consequence of this factor is that high-angle reflections have much less weight in the Fourier series for $\Delta\bar{\phi}(\mathbf{r})$ than they do in the similar expression for $\Delta\bar{\rho}(\mathbf{r})$, such that given an X-ray data set of finite resolution, $\Delta\bar{\phi}(\mathbf{r})$ will be more faithfully represented than $\Delta\bar{\rho}(\mathbf{r})$. Conversely, however, low-angle data become even more significant in retrieving $\Delta\bar{\phi}(\mathbf{r})$, and care needs to be taken in mineral systems to ensure that extinction has been experimentally minimized or that an accurate extinction correction to $|F_o|$ can be made.

As shown in Equation 1, the electrostatic potential includes contributions not only from the electron distribution but also from the distribution of nuclear charge. A Fourier-series expression similar to Equation 3 for the total electrostatic potential, $\phi(\mathbf{r})$, is made tricky by the necessity to include in the structure factor the contributions from the nuclei. Even more serious is the singularity in the $F(000)$ term arising from the $(\sin\theta/\lambda)^{-2}$ factor. Rather than attempt a direct approach, the properties of the electrostatic potential allow one to approximate $\phi(\mathbf{r})$ using a combination of Fourier-series and direct-space methods with no significant loss of accuracy.

It turns out that at distances of about 1 Å from a nucleus, $\phi(\mathbf{r})$ is essentially unaffected by the vibrational motion of the nuclei. In other words, in the extranuclear regions of the crystal, $\phi(\mathbf{r})$ and $\bar{\phi}(\mathbf{r})$ are virtually identical (Spackman and Stewart, 1981). Since the electrostatic potential in the vicinity of an atomic nucleus is totally dominated by the nuclear potential, $\phi(\mathbf{r})$ is of real interest only in regions far removed from the nuclei. It is therefore a valid approximation to include the nuclei in the calculation as static, devoid of any vibrational motion.

In the first term of Equation 3, the Fourier coefficients of vibrationally averaged independent atoms were subtracted away to leave the mean thermal-deformation potential, $\Delta\bar{\phi}(\mathbf{r})$. To obtain the property of interest, the total electrostatic potential, it is necessary to add these independent atoms back in. With virtually no loss of accuracy in the extranuclear regions, this may be accomplished at infinite resolution by a direct-space lattice summation giving rise to the second term in Equation 2. The spherically averaged atomic-density functions included in the direct-space calculation are taken as static, devoid of vibrational motion, and are obtained from the Hartree-Fock wavefunctions of Clementi and Roetti (1974).

In a neutral molecule, the integral of the electrostatic potential over all space must vanish. The same is true for a crystal when considered as a giant molecule. In the same spirit as the Ewald convention for calculating cohesive energies of ionic crystals, it is required that

$$\int_{\text{cell}} \phi(\mathbf{r})\, d\tau = 0, \tag{4}$$

which constrains the unit cell to be electrostatically neutral. The last term in Equation 3 is a constant for the crystal and ensures that the boundary condition of Equation 4 is met.

The electrostatic potential of a crystal obtained by this method is similar to any property obtained from an X-ray diffraction experiment in that it represents an average over the sample crystal. Spectroscopic methods are preferred for probing local structural features; however, a local electron density or electrostatic potential cannot be retrieved from these methods. The influence of defects on local electrostatic properties may in principle be obtained from a theoretically derived electron-density distribution if an appropriate level of theory can be reached. Calculations of this type on a silicate mineral would require obtaining the many-electron wavefunction for the crystal by an SCF calculation to at least the Hartree-Fock level with a large basis. Such calculations are largely intractable and are certainly not commonplace. Although the experimental method outlined above is not ideal, it is the best method currently available for obtaining the electrostatic potential of a crystal that is not biased by some a priori choice of an electron distribution.

Results

The published set of X-ray structure-factor moduli reported by Horiuchi and Sawamoto (1981) consists of a unique set of 675 reflections out to $\sin\theta/\lambda = 1.3$ Å^{-1} scaled by the independent atom model. Of these data, 237 reflections were flagged by Horiuchi and Sawamoto (1981) as having $|F_o| < 3\sigma(|F_o|)$ and were not included in the refinements of this study. Since estimated standard deviations (esd's) in $|F_o|$ were not reported by Horiuchi and Sawamoto (1981), observations were weighted by the reflection multiplicity. A conventional structure refinement wherein scale-factor, positional, and vibrational parameters were varied was completed using the 438 observations reported by Horiuchi and Sawamoto (1981), yielding a scale factor of 0.992(3) and bond lengths and angles that agree to within 1 esd of their results.

In general, when atomic scattering factors are factored into core and valence parts, it is found that valence electrons contribute very little to the scattering at high angles. Since the distribution of core electrons is little affected by chemical bonding, it is assumed that the independent atom model is more realistic for high-order than low-order data. In the so-called X-X method of electron-density mapping, the scale factor, positional parameters, and vibrational parameters used in phasing $|F_o|$ are taken from a refinement using only the high-order data. Such a high-order refinement was completed using data with $\sin\theta/\lambda > 0.65$, resulting in bond lengths and angles within 1

esd of the result using all data, although some vibrational parameters differed by nearly 2 esd's. With only the high-angle weak reflections included, the high-order refinement was not as precise as the full-data result, and a positive correlation between the scale factor and vibrational parameters was observed.

Variations in both the scale factor and vibrational parameters affect the electrostatic potential almost exclusively near the nuclear positions (Spackman and Stewart, 1981). As a consequence of this dependence, electrostatic-potential maps computed using the high-order and full-data parameters were found to be virtually identical. The maps in Figure 2 were computed by using the high-order refinement parameters for F(IAM) and only data which Horiuchi and Sawamoto (1981) found to have $|F_o| > 3\sigma(|F_o|)$. Maps computed using all data are qualitatively similar to those given here and lead to the same conclusions. Least-squares refinements and electrostatic potential mapping were completed using the VALRAY system (Stewart and Spackman, 1983).

Figure 2a shows the electrostatic potential for a plane paralleling (100) containing the bonding plane of O(2) and the Mg(2)–O(1) bond. Small dashes map out electronegative equipotential contours and show where a positive test charge would be attracted by the total charge distribution. Solid contours are electropositive and have been mostly omitted since they rise to a great maximum only at the nuclei, and furthermore, the potential derived from X-ray diffraction data is really informative only in the extranuclear regions. The zero contours are shown by large dashes and are adjacent to the first solid contour. The contour interval is 0.1 e/Å. Chemical bonds are represented by lines drawn between nuclei (plus signs) that are exactly in the mapping plane. Other plus signs show where nuclei that are as much as 1.5 Å out of the plane project onto the mapping plane. For example, the plus signs between Mg(1) and Mg(2) show where the O(4) atoms, which form the shared-edge between Mg(1) and Mg(2) octahedra, project from 1.46 Å above and below the map.

One interesting feature of electrostatic-potential maps of oxides is that cations appear larger than anions, confirming the notion first expressed by Pauling (1928) that the nature of atomic radii depend entirely upon the physical property from which they are derived. Most radii, including Pauling's, are derived from experimental interatomic distances and are thus best suited for predicting bond lengths. However, if one is interested in using radii, for example, to rationalize how a diffusing species interacts with a crystal, then perhaps the electrostatic potential would give a more realistic picture for the sizes of interacting atoms than do traditional radii.

The minima in $\phi(\mathbf{r})$ show where an electrophile would tend to migrate in the Coulomb field of the total charge density. In Figure 2a, these minima are seen on either side of O(3), adjacent to O(1) near the Mg(2)–O(1) bond, and below O(1) on the side opposite Mg(2). The fact that minima in the electrostatic potential appear to cluster

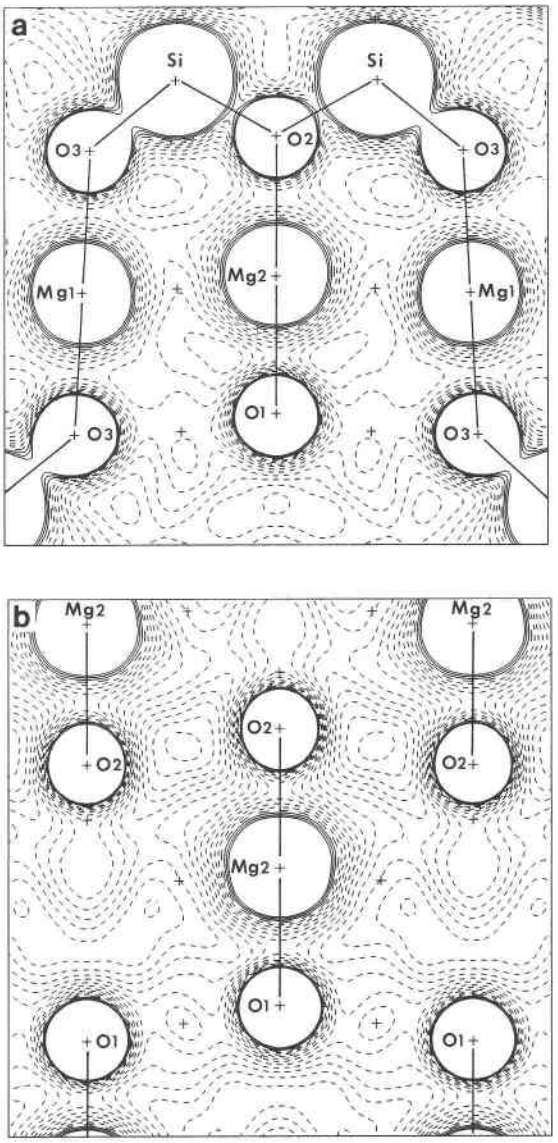

Fig. 2. Electrostatic potential for β-Mg_2SiO_4 derived from X-ray diffraction data. Electronegative contours dashed, electropositive contours solid and not plotted near nuclei. Contour interval is 0.1 e/Å = 1.44 eV/unit charge. (**a**) Plane parallel to (100); (**b**) plane parallel to (010).

around oxygen atoms indicates, as anticipated, that oxygen is more electronegative than Si or Mg. The potential valleys on either side of the Mg(2)–O(1) bond are seen to approach the O(1) side of the bond midpoint, suggesting that the Mg(2)–O(1) bond itself may be a likely candidate for electrophilic attack.

By analogy with molecular systems, the lowest potential minimum in Figure 2a, and therefore the most likely site for protonation, is just below O(1) with a value of -14.9 eV/unit charge. This large feature is located at the base of the square pyramidal coordination polyhedron of O(1). If O(1) were to achieve octahedral coordination by

adding another cation, it would need to be added near the position of this minimum. Although one of the minima adjacent to O(3) is nearly as deep, it is not nearly as extensive as the feature below O(1). This result confirms the suggesstion made by Smyth (1987) and McMillan et al. (1987) that O(1) is a good candidate to be replaced by OH^-.

Figure 2b shows a map of the electrostatic potential for a vertical plane through the center of Figure 2a, parallel to (010), perpendicular to the coordination triangle of O(2), and containing the O(2)–Mg(2)–O(1) linkage. The broadest potential minimum is again adjacent to O(1) on the side opposite the Mg(2)–O(1) bond. In this section the minimum behind O(1) is split into two minima of -16.0 eV/unit charge, whereas over most of this potential valley, the value is about -1 e/Å $= -14.4$ eV/unit charge.

The most interesting result from Figure 2b is that the lowest potential minimum is not associated with O(1) but is on either side of O(2) with a value of -19.4 eV/unit charge. Mapping on a three-dimensional grid at increments of 0.1 Å throughout the asymmetric portion of the unit cell reveals that the minimum associated with O(2) is in fact the global minimum for the unit cell. Although this feature is not as extensive as that associated with O(1), it is much deeper, indicating that as far as the electrostatic potential is concerned, protons situated between O(2) atoms are just as likely as protonation of O(1). Defects wherein hydrogen bonds form between adjacent O(2) atoms would appear to be a possibility. As indicated by Smyth (1987) using ionic-model arguments, O(1) satisfies all of the criteria to be a hydroxyl site. By the same arguments, O(2), which is already formally overbonded, would be highly unlikely candidate for protonation. However, Smyth (1987) evaluated ionic-model site potentials only at the positions of the nuclei and did not attempt to map the electrostatic potential throughout the unit cell from his ionic model. Furthermore, a simple ionic model may not include the charge-density deformations that are likely to give rise to the minima adjacent to O(2). Electrostatic-potential features arising from nonspherical electron-density deformations are only to be seen via accurate electronic-structure calculations or the analysis of X-ray diffraction data.

The minima flanking O(2) in Figure 2b are nearly directly above and below the triangular coordination plane of O(2), which is bonded to two Si and Mg(2). These look very similar to those in the electrostatic potential mapped in the vicinity of the triangularly coordinated oxgyens in stishovite reported by Spackman et al. (1987). The stishovite data are more accurate and extensive than the data used in this study, and therefore, not only the electrostatic potential but also the electron density of stishovite were obtained to high resolution. In stishovite, the largest features in the electron-density deformation are not along the Si–O bond but are above and below the plane of the three-coordinated oxygen and are relatively close to the nucleus. Spackman et al. (1987) have pointed out that these features in stishovite are similar to electron-density deformations observed around two-coordinated oxygens in the disilicic acid molecule as the Si–O–Si angle is opened from 137° to 180° (Geisinger et al., 1987). Although the Horiuchi and Sawamoto data set is not adequate for examining the details of the electron-density distribution, particularly features that peak close to the nuclei, a plausible explanation for the electrostatic-potential minima above and below the bonding plane of O(2) in Figure 2b is that they arise from nonbonded electron-density accumulations analogous to those in stishovite.

If one's vantage point is limited to a strict ionic model governed by Pauling's rules, then the notion that the already overbonded O(2) could accept a proton seems highly implausible. However, by these same criteria, the observed bonding of O(2) to one Mg and two Si also appears anomalous, not to mention the structures of such common minerals as diopside and sillimanite. The fact that formally overbonded anions tend to be involved in long bonds suggests that O(2) may not really be overbonded in the first place. The same argument against protonation of O(2) could be used for the bridging oxygen of the disiloxy group, Si–O–Si, since this oxygen has its valence perfectly satisfied. Ab initio SCF calculations by Geisinger et al. (1985) yield a minimum-energy geometry for disilicic acid, $H_6Si_2O_7$, of 1.591 Å for the bridging bond length and 143.7° for the bridging angle. When a proton was added to the bridging oxygen to form $H_7Si_2O_7^+$, the bridging bond lengthened to 1.709 Å and the angle narrowed to 132.2°, not unlike the geometry of the disiloxy group in β-Mg_2SiO_4. Both disilicic acid and its protonated form are stable molecules in the SCF sense.

Although Horiuchi and Sawamoto (1981) reported 3% vacancies on the Mg(1) site, their crystal was synthesized from presumably dry starting materials and is therefore assumed to contain no OH^- or at least an amount that would go totally unnoticed during analysis of the X-ray data. The maps reported herein are therefore assumed to represent the electrostatic potential of a pure crystal (i.e., without H^+).

It is generally assumed that protonation of O^{2-} in a silicate to form OH^- must be accompanied by a charge-compensating defect, such as the local substitution of a cation of lower charge or a cation vacancy. Smyth (1987) has pointed out that the most probable charge-compensating defects in β-Mg_2SiO_4 would be Mg vacancies. In order to assess the effect that a localized Mg vacancy might have on the observed electrostatic potential, the maps of Figure 2 were recalculated with localized Mg(1), Mg(2), or Mg(3) vacancies. For example, an Mg(1) vacancy was modeled by removing a single Mg(1) independent atom from the lattice sum in the second term of Equation 1. This of course is only an approximation to a real vacancy since the structure is not allowed to relax and no electronic rearrangement is included. When Mg(1) or Mg(2) are removed, the vacant site becomes more electronegative than the minimum near O(1), even though the latter feature is unchanged. The removal of Mg(3) very slightly perturbs the potential minimum around nearby O(1) at-

oms. In every case, the minimum associated with O(2) remains the global minimum in the unit cell.

Conclusions

Experimentally derived electrostatic-potential maps for β-Mg_2SiO_4 corroborate the studies of Smyth (1987) and McMillan et al. (1987) who have suggested that the O(1) site of β-Mg_2SiO_4 could be a host for OH^- in the lower part of the upper mantle. Although the electrostatic-potential minimum associated with the O(1) site is the most extensive in the unit cell, minima above and below the bonding plane of O(2) are deeper by approximately 3.6 eV/unit charge, indicating that protonation processes could take place at O(2) as well as at O(1). These results suggest that nonspherical electron-density deformations may be critical in determining the form of the electrostatic potential and cannot be neglected in theoretical models.

The methods used in this study cannot address the defect structure of β-Mg_2SiO_4, nor can they be used to detect whether H^+ is actually present. These methods can be viewed as one step toward a refinement of the crystal-chemical method utilized by Smyth (1987) in that instead of assuming an ionic model to obtain electrostatic potentials at nuclear positions, the actual electrostatic potential is retrieved from X-ray diffraction data. Polarized IR spectroscopy on a good-quality single crystal with significant H content is necessary to further probe O(1) and O(2) as possible protonation sites. It would also be highly useful to be able to compare these results with electrostatic potentials obtained from electronic-structure calculations or calculations where an electron-density model is assumed (e.g., MEG ionic model). If X-ray structure factors were made available from these calculations, then electrostatic properties could be derived by the same methods used for experimental X-ray diffraction data, thus making possible meaningful comparisons between theory and experiment.

Acknowledgments

I wish to recognize R. F. Stewart of the Chemistry Department at Carnegie-Mellon University for introducing the electrostatic potential to crystallographers and for his pioneering work on the electrostatic potentials of minerals in collaboration with Mark A. Spackman. I am grateful to Charles W. Burnham and an anonymous referee for critical reviews of the manuscript. This research was supported by NSF grant EAR-8618834.

References cited

Bragg, W.L. (1930) The structure of silicates. Zeitschrift für Kristallographie, 74, 237–305.

Burnham, C.W. (1985) Mineral structure energetics and modeling using the ionic approach. In S.W. Kieffer and A. Navrotsky, Eds., Microscopic to macroscopic: Atomic environments to mineral thermodynamics. Mineralogical Society of America Reviews in Mineralogy, 14, 347–388.

Clementi, E., and Roetti, C. (1974) Roothaan-Hartree-Fock wavefunctions: Basis functions and their coefficients for ground and certain excited states of neutral and ionized atoms, $Z < 54$. Atomic Data and Nuclear Data Tables, 14, 177–478.

Downs, J.W., and Gibbs, G.V. (1987) An exploratory examination of the electron density and electrostatic potential of phenakite. American Mineralogist, 72, 769–777.

Geisinger, K.L., Gibbs, G.V., and Navrotsky, A. (1985) A molecular orbital study of bond length and angle variations in framework structures. Physics and Chemistry of Minerals, 11, 266–283.

Geisinger, K.L., Spackman, M.A., and Gibbs, G.V. (1987) Exploration of structure, electron density distribution, and bonding in coesite with Fourier and pseudoatom refinement methods using single-crystal X-ray diffraction data. Journal of Physical Chemistry, 91, 3237–3248.

Horiuchi, H., and Sawamoto, H. (1981) β-Mg_2SiO_4: Single-crystal X-ray diffraction study. American Mineralogist, 66, 568–575.

McMillan, P., Smyth, J.R., and Akaogi, M. (1987) OH in β-Mg_2SiO_4 (abs.). EOS, 68, 1456.

Moore, P.B., and Smith, J.V. (1970) Crystal structure of β-Mg_2SiO_4: Crystal-chemical and geophysical implications. Physics of the Earth and Planetary Interiors, 3, 166–177.

Pauling, L. (1928) The sizes of ions and their influence on the properties of salt-like compounds. Zeitschrift für Kristallographie, 67, 377–404.

Politzer, P., and Truhlar, D.G. (1981) Introduction: The role of the electrostatic potential in chemistry. In P. Politzer and D.G. Truhlar, Eds., Chemical applications of atomic and molecular electrostatic potentials, p. 1–6. Plenum Press, New York.

Smyth, J.R. (1987) β-Mg_2SiO_4: A potential host for water in the mantle? American Mineralogist, 72, 1051–1055.

Smyth, J.R., and Bish, D.L. (1987) Crystal structures and cation sites in the rock-forming minerals, 348 p. Allen & Unwin, London.

Spackman, M.A., and Stewart, R.F. (1981) Electrostatic potentials in crystals. In P. Politzer and D.G. Truhlar, Eds., Chemical applications of atomic and molecular electrostatic potentials, p. 407–425. Plenum Press, New York.

Spackman, M.A., and Weber, H.P. (1988) Electrostatic potential in dehydrated sodium zeolite A from low-resolution X-ray diffraction data. Journal of Physical Chemistry, 92, 794–796.

Spackman, M.A., Hill, R.J., and Gibbs, G.V. (1987) Exploration of structure and bonding in stishovite with Fourier and pseudoatom refinement methods using single crystal and powder X-ray diffraction data. Physics and Chemistry of Minerals, 14, 139–150.

Stewart, R.F. (1979) On the mapping of electrostatic properties from Bragg diffraction data. Chemical Physics Letters, 65, 335–342.

——— (1982) Mapping electrostatic potentials from diffraction data. Godisnjak Jugoslavenskog Centra za Kristalografiju, 17, 1–24.

Stewart, R.F., and Spackman, M.A. (1983) VALRAY Users Manual. Department of Chemistry, Carnegie-Mellon University, Pittsburgh, Pennsylvania.

Tomasi, J. (1981) Use of the electrostatic potential as a guide to understanding molecular properties. In P. Politzer and D.G. Truhlar, Eds., Chemical applications of atomic and molecular electrostatic potentials, p. 1–6. Plenum Press, New York.

Manuscript received October 10, 1988
Manuscript accepted May 24, 1989